Traveling-Wave Protection Method for Boundaryless VSC-HVDC Grids

Mingxuan Tang, Yuqing Wu, Yi Shen, Zhenting Zhao, Yinhong Li
State Key Laboratory of Advanced Electromagnetic Technology
School of Electrical and Electronic Engineering, Huazhong University of Science and Technology
Wuhan, China
email: tang_mingxuan@hust.edu.cn

***Abstract*—With the development of Voltage Source Converter based High Voltage Direct Current (VSC-HVDC) grids from boundary-based to boundaryless configurations, traditional boundary-dependent traveling-wave protection methods become ineffective in boundaryless grids. To address this challenge, this paper proposes a novel traveling-wave protection method suitable for boundaryless grids. The method employs the Ratio of the Integrals of Modal Current Components (RIMCC) to identify internal and external faults. Theoretical analysis of current traveling-wave propagation in boundaryless grids demonstrates that RIMCC exhibits characteristics of distance dependence, boundary distinction, and resistance immunity. Based on these properties, a novel protection method is proposed, with significant advantages in identifying high-resistance faults in boundaryless DC grids while guaranteeing the protection speed. A four-terminal DC grid model is built in PSCAD/EMTDC to verify the effectiveness and performance of the proposed method.**

***Index Terms*—HVDC transmission, traveling-wave protection, boundaryless DC grid, RIMCC, transition resistance**

I. Introduction

Voltage Source Converter based High Voltage Direct Current (VSC-HVDC) grids offer flexible power control, efficient long-distance transmission, and enhanced energy utilization, thus becoming a promising architecture for future power systems [1]. However, compared with AC grids, DC systems suffer from fast-rising fault currents and higher fault probabilities, posing serious challenges to system stability and protection reliability [2], [3]. Traveling-wave protection methods have become the primary protection of the VSC-HVDC grids since they meet the protection speed requirements [4], [5].

Most existing VSC-HVDC grids are boundary-based, where DC reactors are placed at the end of the lines. As HVDC systems evolve into multi-terminal and meshed configurations, reactors are now installed at the converter station outlets to reduce power losses and improve controllability. This results in boundaryless topologies, where distinct line boundaries no longer exist. Consequently, traveling waves no longer exhibit strong reflections at line junctions, and traditional boundary-dependent methods fail to distinguish internal from external faults accurately.

Previous studies have explored various protection strategies for boundaryless grids. In [6], a mathematical morphology–based method achieved tolerance to 300 Ω transition resistance but required an extremely high sampling rate. The approach in [7] combined current-wave integration with voltage rate of change, tolerating only up to 200 Ω. A method in [8] introduced a resistance compensation coefficient for improved tolerance but showed detection delays exceeding 5 ms for remote faults.

To overcome these limitations, this paper proposes a novel traveling-wave protection method using the Ratio of Modal Components of Current Integrals (RIMCC). The RIMCC exhibits clear distance dependence, boundary distinction, and resistance tolerance, enabling accurate Single-Pole-to-Ground (SPTG) fault identification. Simulation results based on a four-terminal PSCAD/EMTDC model verify the fast, selective, and robust performance of the proposed method, demonstrating strong engineering potential.

II. HVDC Transmission System

A typical topology of a boundaryless four-terminal VSC-HVDC transmission system [9]– [11] is illustrated in Fig. 1. In contrast to conventional HVDC grids with distinct boundaries, current-limiting reactors are placed at the converter station outlets instead of line ends. Consequently, the traveling-wave characteristics associated with line boundaries cannot be exploited to distinguish between internal and external faults.

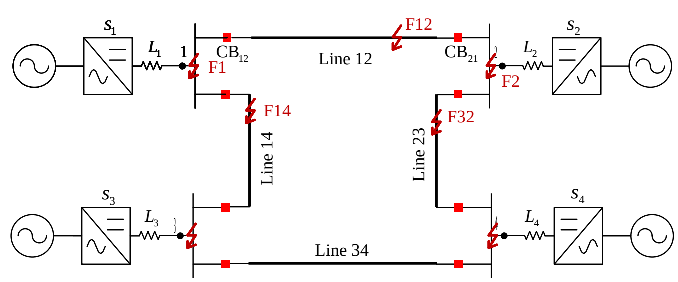

Fig. 1. Boundaryless four-terminal HVDC transmission system

III. Traveling-Wave Propagation Characteristics in Boundaryless HVDC Grids

When a fault occurs on a line in a boundaryless HVDC grid, the forward and backward traveling wave components will be generated. These waves are reflected and refracted at impedance discontinuities such as line terminals or fault points.

979-8-3315-8138-1

Further analysis of the transient process can be performed using the Peterson equivalent circuit, as shown in Fig. 2. Based on this model, reflection and refraction coefficients at each port can be derived. L_s and C_s denote the equivalent inductance and capacitance of the converter station, respectively; L_t is the DC inductance; R_f is the fault transition resistance; k represents the number of parallel branches at the line terminal, which equals 2 in a four-terminal VSC-HVDC system.

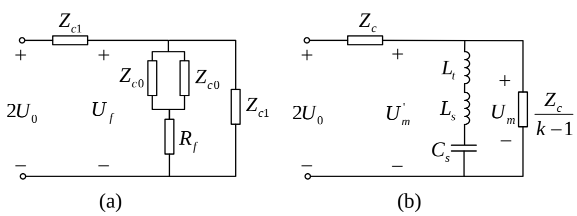

Fig. 2. Peterson equivalent circuit of a boundaryless DC grid:(a) fault point; (b)line terminal

According to the Peterson equivalent circuit of the boundaryless HVDC grid, the transmission and reflection coefficients at the fault port, denoted as α_0 and β_0, can be derived as

$$\alpha_0 = \frac{U_f}{U_0} = \frac{Z_{c0} + 4R_f}{Z_{c1} + Z_{c0} + 4R_f} \tag{1}$$

$$\beta_0 = \alpha_0 - 1 = -\frac{Z_{c1}}{Z_{c1} + Z_{c0} + 4R_f} \tag{2}$$

The converter station branch can be further simplified by analyzing the impedance ratio between its inductive and capacitive elements. The ratio of the inductive to capacitive impedance magnitudes $k_c = |j\omega L_{\text{sum}}/(1/j\omega C_s)|$, ω is the angular frequency, the total equivalent series inductance is $L_{\text{sum}} = L_t + L_s$. For high-frequency transient components, the capacitive effect of C_s becomes negligible.

Based on this simplified model, the transmission and reflection coefficients at the line terminal, α_m amd β_m, are given by

$$\alpha_m = \frac{U_m}{U_0} = \frac{2sL_{\text{sum}}}{ksL_{\text{sum}} + Z_c} \tag{3}$$

$$\beta_m = \alpha_m - 1 = \frac{(2-k)sL_{\text{sum}} - Z_c}{ksL_{\text{sum}} + Z_c} \tag{4}$$

During propagation, traveling waves undergo attenuation and dispersion. For an internal positive-pole ground fault in a four-terminal VSC-HVDC system, the current components measured at the protection terminal [5] can be expressed as

$$\begin{cases} i_{in\_i}(s) = (1-\beta_m)e^{-a_i x}e^{-\frac{sx}{v_i}}\dfrac{i_{fi}}{s} \\ i_{in\_i}(t) = i_{fi}e^{-a_i x}(2 - e^{-\frac{Z_{ci}}{2L_{\text{sum}}}(t-\frac{x}{v_i})})u(t - \dfrac{x}{v_i}) \end{cases} \tag{5}$$

where $i_{in\_i}(s)$ $(i = 1, 0)$ represent the frequency-domain internal fault current components measured at the protection location; $i_{in\_i}(t)$ $(i = 1, 0)$ represent the time-domain internal fault current components measured at the protection location; Z_{ci} $(i = 1, 0)$ denote the characteristic impedances for the line-mode and ground-mode components; a_i $(i = 1, 0)$ are the attenuation coefficients of the line-mode and ground-mode components; t is the time after the fault occurrence; x is the fault distance; v_i $(i=1,0)$ are the propagation velocities of the line-mode and ground-mode components; and i_{fi} $(i=1,0)$ are the current traveling waves at the fault point for the line-mode and ground-mode.

For an external positive-pole ground fault in a four-terminal VSC-HVDC system, the current components measured at the protection terminal can be expressed as

$$\begin{cases} i_{ex\_i}(s) = (1-\beta_m)\alpha_m e^{-a_i x}e^{-\frac{sx}{v_i}}\dfrac{i_{fi}}{s} \\ i_{ex\_i}(t) = i_{fi}e^{-a_i x}\left(1 + \dfrac{Z_{ci}}{2L_{\text{sum}}}\left(t - \dfrac{x}{v_i}\right)\right) \\ \qquad \cdot e^{-\frac{Z_{ci}}{2L_{\text{sum}}}\left(t-\frac{x}{v_i}\right)} u\left(t - \dfrac{x}{v_i}\right) \end{cases} \tag{6}$$

where $i_{ex\_i}(s)$ $(i = 1, 0)$ represent the frequency-domain external fault current components measured at the protection location; $i_{ex\_i}(t)$ $(i = 1, 0)$ represent the time-domain external fault current components measured at the protection location.

IV. Definition, Calculation, and Characteristics of RIMCC

In boundaryless HVDC grids, high-resistance faults are typically SPTG faults. To effectively identify these faults, RIMCC method is proposed, which enables rapid and accurate discrimination between internal and external faults, while exhibiting strong robustness against high transition resistance.

A. Definition of RIMCC

When a SPTG fault occurs on the line, the line-mode and ground-mode current traveling-wave waveforms at the protection measurement point are shown in Fig. 3. Within the time window, the integral values of the line-mode and ground-mode current traveling waves are represented by the shaded areas in the figure.

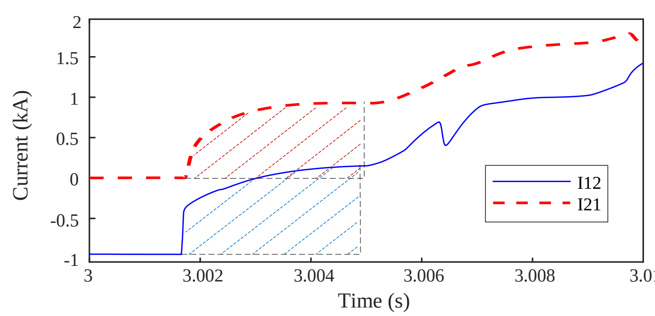

Fig. 3. Line-mode and ground-mode current traveling waves

In this paper, RIMCC is defined as the ratio of the integral values of the line-mode and ground-mode current traveling waves within the time window, expressed as

$$\text{RIMCC} = \frac{\int_{t_1}^{t_1+T} i_{R1}(t)\text{d}t}{\int_{t_0}^{t_0+T} i_{R0}(t)\text{d}t} \tag{7}$$

979-8-3315-8138-1

where t_i $(i = 1, 0)$ are the arrival times of the line-mode and ground-mode current components; T is the length of the time window; $i_{Ri}(t)$ $(i = 1, 0)$ are the fault current components measured at the protection location.

B. Theoretical Calculation of RIMCC

For internal faults, RIMCC can be expressed as

$$\begin{aligned}\text{RIMCC} &= \frac{i_{f1}}{i_{f0}}\frac{e^{-a_1 x}}{e^{-a_0 x}}\frac{\int_{t_1}^{t_1+T}(2-e^{-\lambda_1(t-t_1)})u(t-t_1)\mathrm{d}t}{\int_{t_0}^{t_0+T}(2-e^{-\lambda_0(t-t_0)})u(t-t_0)\mathrm{d}t} \\ &= \frac{i_{f1}}{i_{f0}}\frac{2T+\frac{1}{\lambda_1}(e^{-\lambda_1 T}-1)}{2T+\frac{1}{\lambda_0}(e^{-\lambda_0 T}-1)}e^{-(a_1-a_0)x}\end{aligned} \tag{8}$$

where $\lambda_i = Z_{ci}/2L_{\text{sum}}$ $(i = 1, 0)$ are the constant coefficients of the line-mode and ground-mode components.

For external faults, RIMCC can be expressed as

$$\begin{aligned}\text{RIMCC} &= \frac{\int_{t_1}^{t_1+T}(1+\frac{Z_{c1}}{2L_{\text{sum}}}(t-\frac{x}{v_1}))e^{-\frac{Z_{c1}}{2L_{\text{sum}}}(t-\frac{x}{v_1})}u(t-t_1)\mathrm{d}t}{\int_{t_0}^{t_0+T}(1+\frac{Z_{c0}}{2L_{\text{sum}}}(t-\frac{x}{v_0}))e^{-\frac{Z_{c0}}{2L_{\text{sum}}}(t-\frac{x}{v_0})}u(t-t_0)\mathrm{d}t} \\ &\cdot \frac{i_{f1}}{i_{f0}}\frac{e^{-a_1 x}}{e^{-a_0 x}} \\ &= \frac{i_{f1}}{i_{f0}}\frac{\frac{2}{\lambda_1}-e^{-\lambda_1 T}(T+\frac{2}{\lambda_1})}{\frac{2}{\lambda_0}-e^{-\lambda_0 T}(T+\frac{2}{\lambda_0})}e^{-(a_1-a_0)x}\end{aligned} \tag{9}$$

Since the attenuation coefficient $a_1 < a_0$ [12], it follows that $e^{-(a_1-a_0)x}$ increases with the fault distance x. Thus, RIMCC increases with the fault distance and is independent of the transition resistance.

By substituting typical parameters of a conventional HVDC system ($Z_{c1} = 377\Omega$, $Z_{c0} = 658\Omega$, $L_{\text{sum}} = 0.0327\text{H}$), the constant term of RIMCC is obtained as $0.96\, i_{f1}/i_{f0}$ for internal faults and $1.72\, i_{f1}/i_{f0}$ for external faults. These results demonstrate that RIMCC exhibits clear boundary distinction characteristics.

C. Characteristic Analysis

Analytical results in Fig 4 show that RIMCC exhibits three key characteristics in boundaryless DC grids:

- **Distance Dependence:** RIMCC increases monotonically with the fault distance from the measurement terminal. Internal faults yield smaller RIMCC values than external ones.
- **Boundary Distinction:** The difference in RIMCC between internal and external faults forms a clear numerical boundary. This provides a reliable quantitative criterion for fault identification.
- **Resistance Immunity:** Transition resistance affects both line-mode and ground-mode wave integrals proportionally, leaving RIMCC almost unchanged. Hence, RIMCC remains stable even under high-resistance faults (up to 800 Ω in simulations).

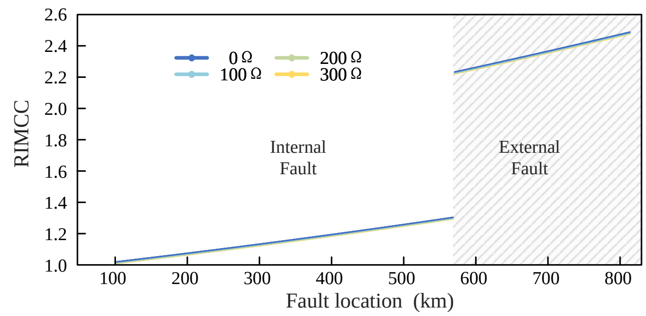

(a) RIMCC values under different fault distances

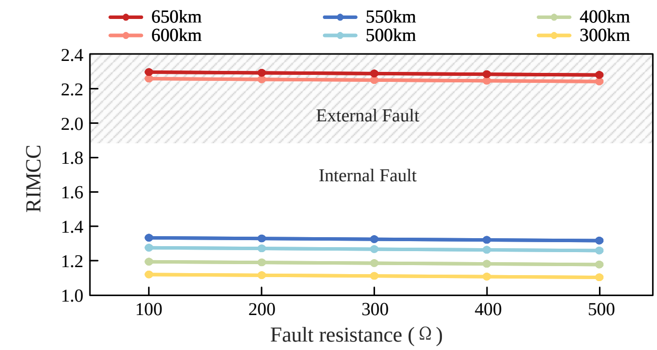

(b) RIMCC values under different transition resistances

Fig. 4. RIMCC values under different fault distances and transition resistances

V. Traveling-Wave Protection Method for Boundaryless HVDC Grids

A. Overall Protection Logic

The protection program flowchart is shown in Fig. 5. After a fault occurs, the protection is first activated by the starting criterion. Once the ground-fault identification criterion detects a SPTG fault, the RIMCC-based criterion is applied to distinguish between internal and external faults, and the pole identification criterion is subsequently used to determine the faulted pole.

B. Protection Method Criteria

1) Protection startup: The protection is triggered when the integral of the voltage drop at the measurement point exceeds a threshold:

$$\int \Delta u_f dt < m_{\text{set}} \tag{10}$$

where Δu_f denotes the fault voltage traveling wave at the protection location; m_{set} is the threshold setting for the startup criterion.

2) Ground-fault Identification: Ground-fault identification is based on the integral of the ground-mode current:

$$\left|\int \Delta i_{f0} dt\right| > \varepsilon_{\text{set}} \tag{11}$$

where Δi_{f0} represents the ground-mode current traveling wave at the protection location; ε_{set} is the threshold setting for the ground-fault identification criterion.

979-8-3315-8138-1

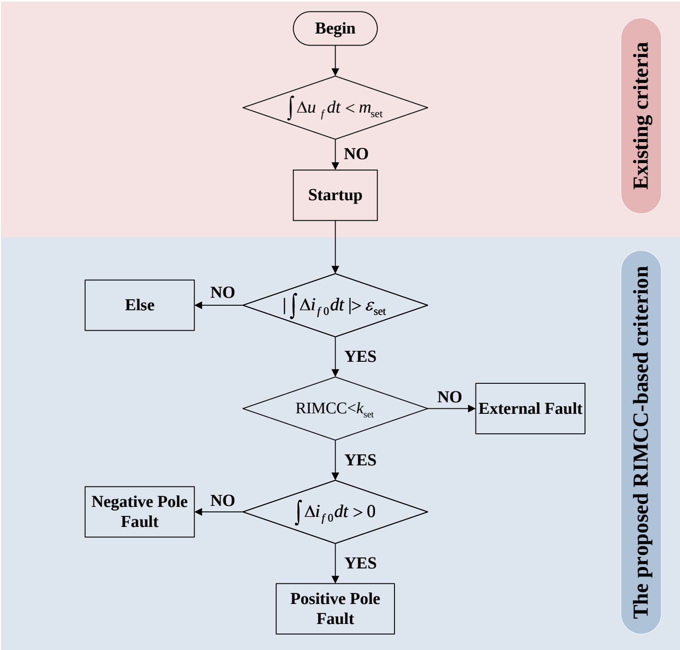

Fig. 5. Protection program flowchart

3) Pole Identification: The polarity of the ground-mode current integral determines whether the fault occurs on the positive or negative pole:

$$\int \Delta i_{f0} dt > 0 \tag{12}$$

4) Internal/external identification: Based on the properties mentioned above, the RIMCC exhibits clear distance dependence, boundary distinction, and strong transition-resistance tolerance. Therefore, the internal and external faults are identified using the following criterion:

$$\text{RIMCC} < k_{\text{set}} \tag{13}$$

where k_{set} denotes the threshold setting for the internal and external fault identification criterion.

5) Other fault identification: The proposed protection method primarily enhances the identification of single-pole-to-ground faults in boundaryless grids. Pole-to-pole faults, which are generally metallic or low-resistance, can still be effectively identified using conventional protection methods [5].

VI. Simulation Verification

To verify the correctness and feasibility of the proposed protection method, a four-terminal HVDC grid model was established in PSCAD/EMTDC, as shown in Fig. 1. The system operates at ±400 kV with a total line length of 600 km. Each converter adopts a modular multilevel converter (MMC) configuration, and the reactors (200 mH) are installed at the converter outlets.

A. Simulation Settings

The sampling frequency is set to 50 kHz to ensure adequate transient capture of the traveling waves. The time window is set to 1 ms, ensuring that the RIMCC primarily includes the first traveling wave. Faults are simulated on Line L12 at various distances and transition resistances to evaluate both the distance and resistance tolerance of the proposed criterion.

The protection setting values are summarized in Table I.

TABLE I
Protection Setting Values

Protection parameters	m_{set}	ε_{set}	k_{set}	n_{set}
Threshold	-10 kV·ms	0.5 kA·ms	1.4	484 kV

B. Results and Analysis

To evaluate the performance of the method, multiple SPTG faults were simulated under varying conditions.

As summarized in Table II, the simulation results confirm that RIMCC exhibits a distinct pattern across all tested cases:

- For internal faults, RIMCC values increase gradually with fault distance but remain below the threshold $k_{\text{set}} = 1.4$.
- For external faults, RIMCC is above 1.5, exceeds the threshold significantly .
- The RIMCC value remains stable across all transition resistances, confirming strong resistance immunity.

C. Operation Speed and Resistance Tolerance

For all tested internal faults, the proposed protection method accurately identified the fault type within 1 ms. During this process, the converter arm currents stayed within twice their rated values, ensuring that no blocking was triggered.

The tolerance of the proposed protection method to transition resistance is verified. There is a significant difference in RIMCC between high-resistance faults at the end of the protected zone and external metallic faults, as shown in the figure 6.

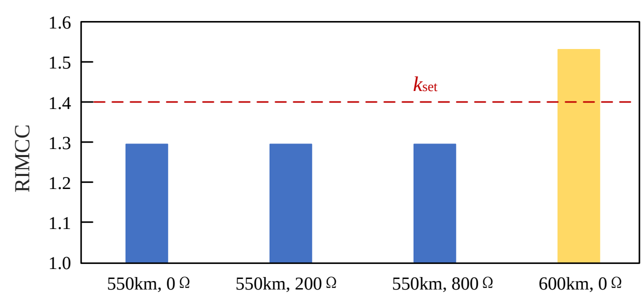

Fig. 6. RIMCC's tolerance to transition resistance

The method maintained reliable operation for transition resistances up to 800 Ω, surpassing the capability of conventional traveling-wave protection schemes.

D. Comparison with Existing Methods

A comparative study was conducted among the proposed RIMCC-based protection, the boundary-based protection [5], the mathematical morphology–based method [6], the first current integration of non-fault pole (FCINP) [7] method,

TABLE II
SIMULATION RESULTS FOR FAULTS AT DIFFERENT LOCATIONS

Fault location	Fault conditions		Fault identification criteria		Fault identification
	Fault type	Transition resistance (Ω)	$\int \Delta i_{f0} > 0$?	RIMCC	Results
100 km	p-g (p)	0	Y	0.977	Positive pole fault
	p-g (n)	0	N	0.972	Negative pole fault
200 km	p-g (p)	0	Y	1.028	Positive pole fault
	p-g (n)	0	N	1.029	Negative pole fault
300 km	p-g (p)	0	Y	1.094	Positive pole fault
	p-g (n)	0	N	1.083	Negative pole fault
400 km	p-g (p)	0	Y	1.157	Positive pole fault
	p-g (n)	0	N	1.156	Negative pole fault
500 km	p-g (p)	0	Y	1.225	Positive pole fault
	p-g (n)	0	N	1.214	Negative pole fault
550 km	p-g (p)	0	Y	1.297	Positive pole fault
	p-g (p)	100	Y	1.293	Positive pole fault
	p-g (p)	200	Y	1.292	Positive pole fault
	p-g (n)	0	N	1.295	Negative pole fault
	p-g (n)	100	N	1.292	Negative pole fault
	p-g (n)	200	N	1.290	Negative pole fault
600 km (External)	p-g (p)	0	Y	1.526	External fault
	p-g (n)	0	N	1.521	External fault

and the resistance-compensation approach [8]. Table III summarizes the performance comparison. The proposed method achieves faster operation time and higher resistance tolerance, while maintaining simple implementation and moderate data requirements.

TABLE III
COMPARISON OF DIFFERENT PROTECTION METHODS

Method	Operation time (ms)	Resistance tolerance (Ω)	Sampling frequency (kHz)
boundary-based [5]	0.8	0	20
Morphology-based [6]	2.8	300	200
FCINP [7]	0.38	200	50
Compensation [8]	5.95	600	10
Proposed RIMCC	1	800	50

VII. CONCLUSION

This paper presents a novel traveling-wave protection method for boundaryless HVDC grids. The proposed RIMCC index exhibits distinct characteristics of distance dependence, boundary distinction, and resistance immunity, enabling reliable discrimination between internal and external faults. Both theoretical analysis and simulation studies verify that the RIMCC-based protection can rapidly and accurately identify fault locations and the faulted pole. Compared with existing methods, the proposed method achieves faster detection, operates at a lower sampling frequency of only 50 kHz, and demonstrates superior tolerance to transition resistance. These advantages highlight the strong potential of the RIMCC-based protection scheme for practical deployment in future DC grids.

REFERENCES

[1] M. Muniappan, "A comprehensive review of DC fault protection methods in HVDC transmission systems," Protection and Control of Modern Power Systems, vol. 6, no. 1, p. 1, 2021.

[2] W. Xiang, S. Yang, G. P. Adam, et al., "DC fault protection algorithms of MMC-HVDC grids: fault analysis, methodologies, experimental validations, and future trends," IEEE Transactions on Power Electronics, vol. 36, no. 10, pp. 11245–11264, 2021.

[3] Y. Zhang, N. Tai, and B. Xu, "Fault analysis and traveling-wave protection scheme for bipolar HVDC lines," IEEE Transactions on Power Delivery, vol. 27, no. 3, 2012.

[4] S. Shi, B. Zhu, A. Lei, et al., "Fault location for radial distribution network via topology and reclosure-generating traveling waves," IEEE Transactions on Smart Grid, vol. 10, no. 6, pp. 6404–6413, 2019.

[5] T. Lan and X. Duan, "High fault-resistance tolerable traveling wave protection for multi-terminal VSC-HVDC," IEEE Transactions on Power Delivery, vol. 36, no. 2, 2021.

[6] N. Tong, X. Lin, X. Zhang, et al., "A boundary-independent local distance traveling-wave protection principle for overhead multi-terminal flexible DC grids," Proceedings of the CSEE, vol. 39, no. 7, pp. 2049–2060, 2019.

[7] Z. Zhao, S. Wu, Y. Shen, et al., "Traveling-wave protection for flexible DC grids with different boundary structures," Proceedings of the CSEE, pp. 1–13, 2024.

[8] T. Chen, Z. Zhao, and Y. Li, "Inverse-time overcurrent protection configuration for flexible DC grids without boundary elements," Power System Protection and Control, vol. 51, no. 16, pp. 48–58, 2023.

[9] M. Kong, X. Pei, H. Pang, et al., "A lifting wavelet-based protection strategy against DC line faults for Zhangbei HVDC grid in China," in Proc. 19th European Conf. on Power Electronics and Applications (EPE'17 ECCE Europe), Warsaw, 2017, pp. 1–11.

[10] Y. M. Yeap and A. Ukil, "Fault detection in HVDC systems using short-time Fourier transform," in Proc. IEEE Power and Energy Society General Meeting (PESGM), 2016, pp. 1–5.

[11] G. Balzer, A. Saciak, A. Wasserrab, et al., "Short-circuit calculation in AC networks in case of HVDC stations with line-commutated converters (LCC)," in Proc. 20th European Conf. on Power Electronics and Applications (EPE'18 ECCE Europe), 2018, pp. 1–9.

[12] S. Lin, Z. He, X. Li, and Q. Qian, "Travelling wave time-frequency characteristic-based fault location method for transmission lines, " IET Gen. Transm. Distrib., vol. 6, no. 8, pp. 764–772, 2012.

979-8-3315-8138-1